Bulletin of the Seismological Society of America, Vol. 104, No. 6, pp. –, December 2014, doi: 10.1785/0120140003

Ⓔ

Late Holocene Slip Rate and Ages of Prehistoric Earthquakes along the Maacama Fault Near Willits, Mendocino County, Northern California

by Carol S. Prentice, Martin C. Larsen,* Harvey M. Kelsey, and Judith Zachariasen

Abstract The Maacama fault is the northward continuation of the Hayward–Rodgers Creek fault system and creeps at a rate of 5.7 ± 0.1 mm/yr (averaged over the last 20 years) in Willits, California. Our paleoseismic studies at Haehl Creek suggest that the Maacama fault has produced infrequent large earthquakes in addition to creep. Fault terminations observed in several excavations provide evidence that a prehistoric surface-rupturing earthquake occurred between 1060 and 1180 calibrated years (cal) B.P. at the Haehl Creek site. A folding event, which we attribute to a more recent large earthquake, occurred between 790 and 1060 cal B.P. In the last 560–690 years, a buried channel deposit has been offset 4.6 ± 0.2 m, giving an average slip rate of 6.4–8.6 mm/yr, which is higher than the creep rate over the last 20 years. The difference between this slip rate and the creep rate suggests that coseismic slip up to 1.7 m could have occurred after the formation of the channel deposit and could be due to a paleoearthquake known from paleoseismic studies in the Ukiah Valley, about 25 km to the southeast. Therefore, we infer that at least two, and possibly three, large earthquakes have occurred at the Haehl Creek site since 1180 cal B.P. (770 C.E.), consistent with earlier studies suggesting infrequent, large earthquakes on the Maacama fault. The short-term geodetic slip rate across the Maacama fault zone is approximately twice the slip rate that we have documented at the Haehl Creek site, which is averaged over the last approximately 600 years. If the geodetic rate represents the long-term slip accumulation across the fault zone, then we infer that, in the last ∼1200 years, additional earthquakes may have occurred either on the Haehl Creek segment of the Maacama fault or on other active faults within the Maacama fault zone at this latitude.

Online Material: Trench logs, discussion of channel B, photographs of compressional features, and table of radiocarbon analyses.

Introduction and Tectonic Setting

Near the northern end of the transform plate boundary, the San Andreas fault system in northern California consists of at least three major fault zones: from west to east, the San Andreas, Maacama, and Bartlett Springs fault zones (Fig. 1a). Geodetic studies indicate that these faults together accommodate up to 86% of the total horizontal plate-boundary motion between the North American and Pacific plates (Freymueller *et al.*, 1999). The geodetic model suggests that the northern San Andreas fault accounts for only about 38% of the plate motion and implies that the Maacama and Bartlett Springs faults together must accommodate significant plate-boundary motion. Our study addresses the late Holocene slip rate for the Maacama fault in Mendocino County at the latitude of Willits, California.

Previous studies of the Maacama fault mapped active traces of the fault between Hopland and Laytonville (Pampeyan *et al.*, 1981; Upp, 1989; Fig. 1b) and demonstrated late Holocene displacement (Upp, 1989). The Maacama fault creeps at the ground surface, and its fastest measured creep rate is in Willits (McFarland *et al.*, 2013; Fig. 1b). The fault traverses the town of Willits, where numerous cultural features show the effects of fault creep (Hecker and Kelsey, 2006; Fig. 2). Repeated measurements of an alignment array near the northern end of the town show a creep rate of 5.7 ± 0.1 mm/yr at the ground surface for the time interval

*Now at Wyoming State Geological Survey, P.O. Box 1347, Laramie, Wyoming 82703.

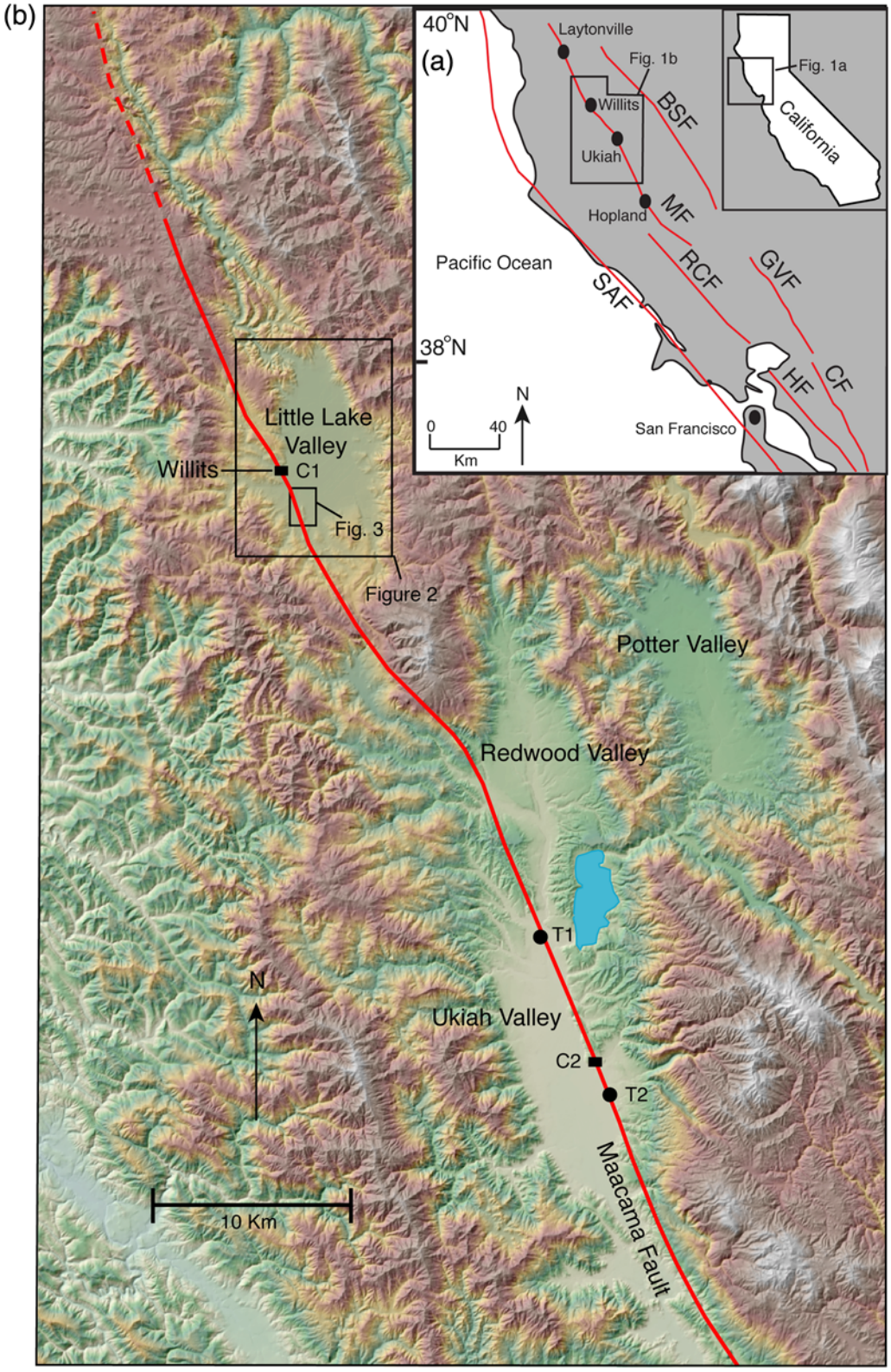

Figure 1. (a) Part of northern California showing locations of the principal plate-boundary fault zones and of panel b. (BSF, Bartlett Springs fault; CF, Calaveras fault; GVF, Green Valley fault; HF, Hayward fault; MF, Maacama fault; RCF, Rodgers Creek fault; SAF, San Andreas fault.) The inset shows the state of California for location. (b) Topographic map from a digital elevation model (DEM) showing the main trace of the Maacama fault, location of Figure 2, and location of the study site southeast of Willits (within the rectangle labeled Figure 3). The solid rectangles show sites where fault creep is measured across alignment arrays in Willits (C1) and in Ukiah Valley (C2) (McFarland *et al.*, 2013). Dots show trench sites of Sickler *et al.* (2005) in the Ukiah Valley area. The color version of this figure is available only in the electronic edition.

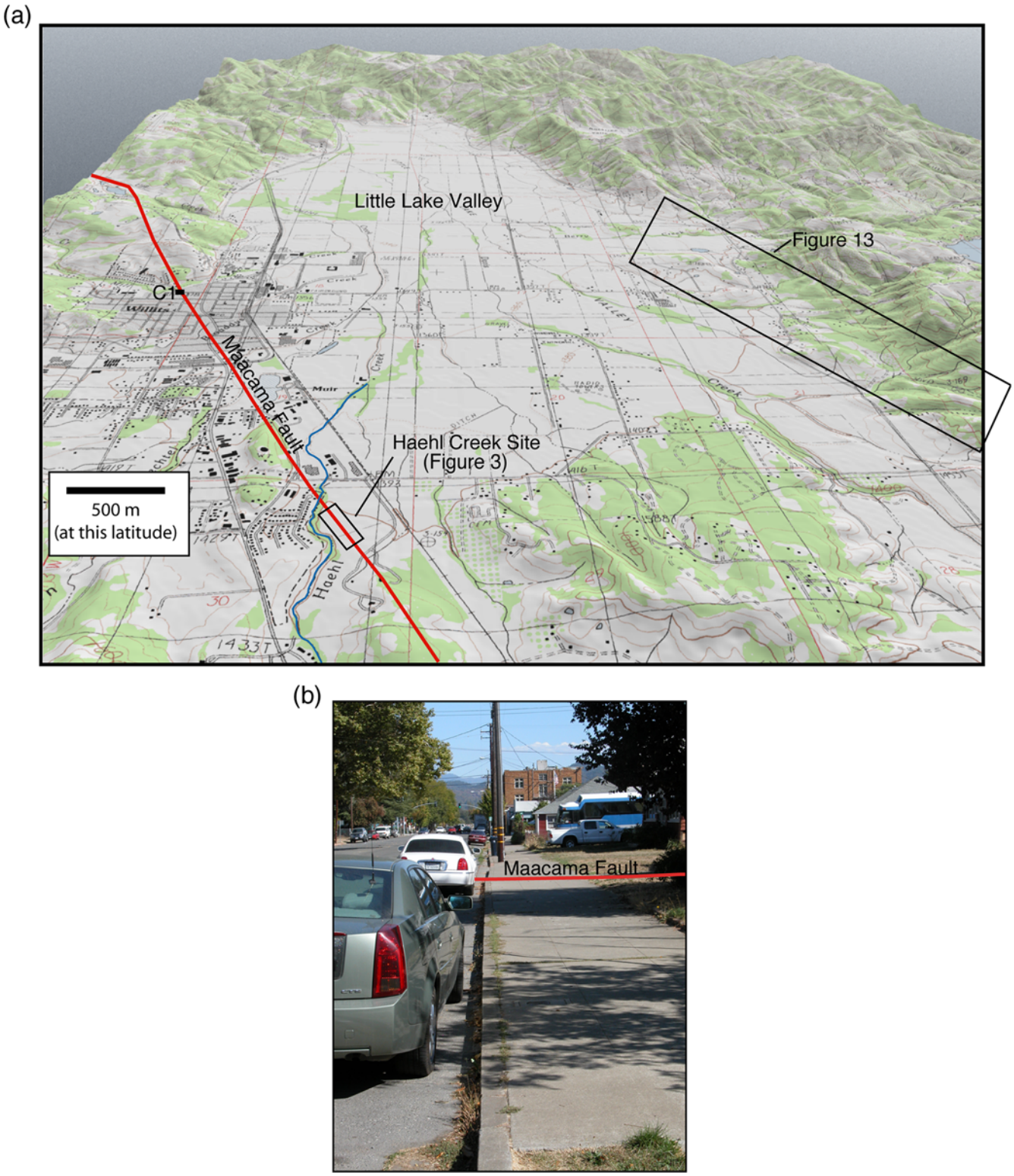

Figure 2. (a) DEM showing an oblique view looking north of Little Lake Valley and the town of Willits. The thick line shows the approximate location of the Maacama fault. C1 is the location of the alignment array where creep is measured on West Commercial Street. (b) The photograph shows an offset curb due to fault creep. The view is eastward, down the south side of West Commercial Street, near C1. The color version of this figure is available only in the electronic edition.

1992–2012 (McFarland *et al.*, 2013). Creep has also been reported, though at the lower rate of 4.3 ± 0.8 mm/yr, farther south in the Ukiah Valley (McFarland *et al.*, 2013), where paleoseismic work suggests that a large prehistoric earthquake occurred between the years 1410 and 1660 C.E. (Sickler *et al.*, 2005).

Microseismicity is abundant in the region of the Maacama fault at the latitude of Willits (Castillo and Ellsworth, 1993). Relocation of hypocenters of seismicity at this latitude (between 39°18′ N and 39°36′ N) indicates that most seismicity along the Maacama fault zone is situated below the eastern part of the Little Lake Valley, at depths of 2–12 km, and is 10 km to the east of the main fault trace that is creeping at the surface (Hayes and Furlong, 2006).

No large historical earthquakes are known to have produced surface rupture in the Willits area (Toppozada *et al.*, 1981), leaving open the question of whether the fault near Willits moves only in creep or whether it releases some slip in large, surface-rupturing earthquakes. Analysis of Global Positioning System (GPS) geodetic data suggests that the modern slip rate across the Maacama fault zone is about 14 mm/yr (Freymuller *et al.*, 1999), which is significantly higher than the measured creep rate at the surface.

Our study was designed to constrain the late Holocene slip rate on the main Maacama fault trace to compare the geologic slip rate to the modern measured creep rate and to the slip rate for the fault zone derived from GPS geodesy. A long-term slip rate close to the measured modern creep rate would imply that most or all strain occurs as creep. However, a long-term slip rate that is significantly higher than the modern creep rate would imply either that the creep rate has varied over the last few thousand years or that some fraction of the total strain is released in surface-rupturing earthquakes.

We excavated both fault-perpendicular and fault-parallel trenches and exposed offset buried channel deposits along the Maacama fault. We exposed the margins of the channels on either side of the fault, measured their offsets, and collected multiple charcoal samples for radiocarbon dating. Additionally, we identified evidence that suggests the occurrence of two prehistoric earthquakes in two of our fault-perpendicular excavations.

Study Site and Methods

The Haehl Creek site is located near the southern end of the city of Willits on the valley floor surface into which Haehl Creek is incised (Figs. 2 and 3). Study of aerial photographs and previous mapping by Pampeyan *et al.* (1981) and Upp (1989) show the main fault trace traversing the Little Lake Valley and crossing the modern channel of Haehl Creek, which is incised about 8 m into the valley floor. Across most of the site, the only surface expression of the Maacama fault is a prominent 4 m high, 140 m long pressure ridge immediately north of our study area (Figs. 3 and 4). Our study is focused on the area south of the ridge where the geomorphology and excavations by geotechnical consultants (SHN Consulting Engineers & Geologists, Inc., 2004a,b) (SHN) suggest that old channels of Haehl Creek once flowed northeastward across the Maacama fault, creating the broad alluvial surface east and south of the pressure ridge.

We excavated eight trenches across and parallel to the Maacama fault (Fig. 5) to expose former channels of Haehl Creek and the fault zone. We located the edges of four distinct gravel bodies (two on each side of the fault) deposited by Haehl Creek (Fig. 6) and followed them in detail up to the fault zone on either side of the fault in order to measure their offsets (Fig. 7). Ⓔ For detailed logs of individual slices, see Figures S1 and S2 in the electronic supplement to this article. Additionally, we collected charcoal samples for radiocarbon dating (Tables 1 and 2). We used two different techniques to follow the channel edges to the fault. (1) In the case of the southern gravel bodies (gravels I and II; Fig. 6), after locating the channel edge several meters away from the fault, we exposed the channel edge in a series of sequential vertical cuts up to the point where the channel intersected the fault zone (Fig. 7). This is similar to the technique used by Wesnousky *et al.* (1991) and Prentice *et al.* (2003). (2) In the case of the northern gravel bodies (gravels III and IV; Fig. 6), we exposed the edges of the gravel deposits in map view and followed them continuously up to the point where the channel edges intersect the fault zone. Ⓔ For photographs and logs of the trench floor showing the edges of these gravel deposits, see Figures S3 and S4.

In the northern part of our study area, between trenches 6 and 8, the Maacama fault is a narrow (1–1.5 m wide), subvertical fault zone striking N34°W (Fig. 5). In the southern part of our study area, we documented a left stepover zone across a 15 m wide, 60 m long area between trench 1 and SHN2 (Fig. 5). South of the stepover, all slip is accommodated by the steeply dipping fault that carries strike-slip displacement to the southeast, which was exposed as a subvertical, narrow fault zone in the southernmost SHN trench (SHN2, Fig. 5; SHN, 2004b). Within the left stepover zone, the fault dip decreases to 36° and is characterized by a significant component of reverse slip, as shown by slickensides exposed in trench 3 that trend N48°E and plunge 48° NE on a fault plane striking N31°W (Larsen, 2006; Ⓔ Fig. S7). In trenches 2 and 3, Pleistocene sedimentary units are thrust over Holocene alluvial deposits, and units are deformed by folding as well as by brittle faulting (Figs. 8 and 9).

Offset Channels

Our excavations exposed four distinct gravel bodies that have been offset by strike-slip displacement. Gravel bodies I and III are exposed about 50 m apart and 5 m west of the fault zone in fault-parallel trench 4, and gravel bodies II and IV are exposed about 30 m apart east of the fault zone in fault-parallel trench 7 (Fig. 6). The gravels are typically characterized by east-dipping foreset beds, indicating an east-northeast flow direction. We infer that northeast-flowing

Figure 3. The oblique aerial photograph looking eastward shows the Haehl Creek site near the southern end of Willits. The low hill is a pressure ridge indicating the location of the fault across the otherwise featureless valley floor into which Haehl Creek is incised. Solid lines show the approximate location of the Maacama fault. Short dashes outline the study site shown in Figure 4. The dashed-dotted line indicates the modern channel of Haehl Creek, which is incised about 8 m into the valley floor. The circle labeled C marks the location of the left-stepping en echelon cracks across East Hill Road that indicate fault creep. The color version of this figure is available only in the electronic edition.

paleochannels of Haehl Creek deposited the gravel bodies across the fault zone.

We collected charcoal samples from the four gravel packages and the surrounding deposits. Radiocarbon dates cluster into two age ranges for the four gravel bodies (Table 1). Based on field relations and the radiocarbon ages, gravels I and II are correlative. Our initial interpretation based on field relations alone was that gravels III and IV would also be correlative; however, the radiocarbon ages do not support this, and instead show that gravel IV is the same age as gravels I and II (Table 1). Radiocarbon ages of gravel III are distinctly older, indicating this deposit is part of an older channel complex. We correlate gravels I, II, and IV as belonging to what we designate channel A, and gravel III as belonging to channel B (Table 1). We conclude that channel A flowed eastward across the fault, then turned to the north before turning again to the east (Fig. 10). The outside bend of the channel intersects the fault and appears in trench 7 as gravel body IV (Fig. 10). Although we originally concluded from field relations that the offset equivalent of channel B is gravel body IV, the radiocarbon ages suggest that the offset equivalent of channel B was eroded away during or prior to the time channel A and its associated deposits were forming. Unfortunately, it is not possible to place any meaningful constraints on the magnitude of the channel B offset. Ⓔ Part 2 of the electronic supplement contains additional discussion about gravels III and IV.

Channel Ages

We dated 22 charcoal samples from channel A and 6 charcoal samples associated with channel B (Table 1). The locations of these samples are shown on the corresponding trench logs (Figs. 6 and Ⓔ S1, S2, S5, and S6). Because detrital charcoal is older than the sediments in which it is deposited, we consider the youngest sample ages within a unit to most closely approximate the age of the deposit. Among the samples collected from channel A, half (11 of 22) fall into the range of 510–760 cal B.P. (designated group 1 on Table 1), and their ages are indistinguishable within the error. Within this group, sample 102 gives the youngest age of 510–640 cal B.P., and we take this age to most closely represent the age of abandonment of channel A.

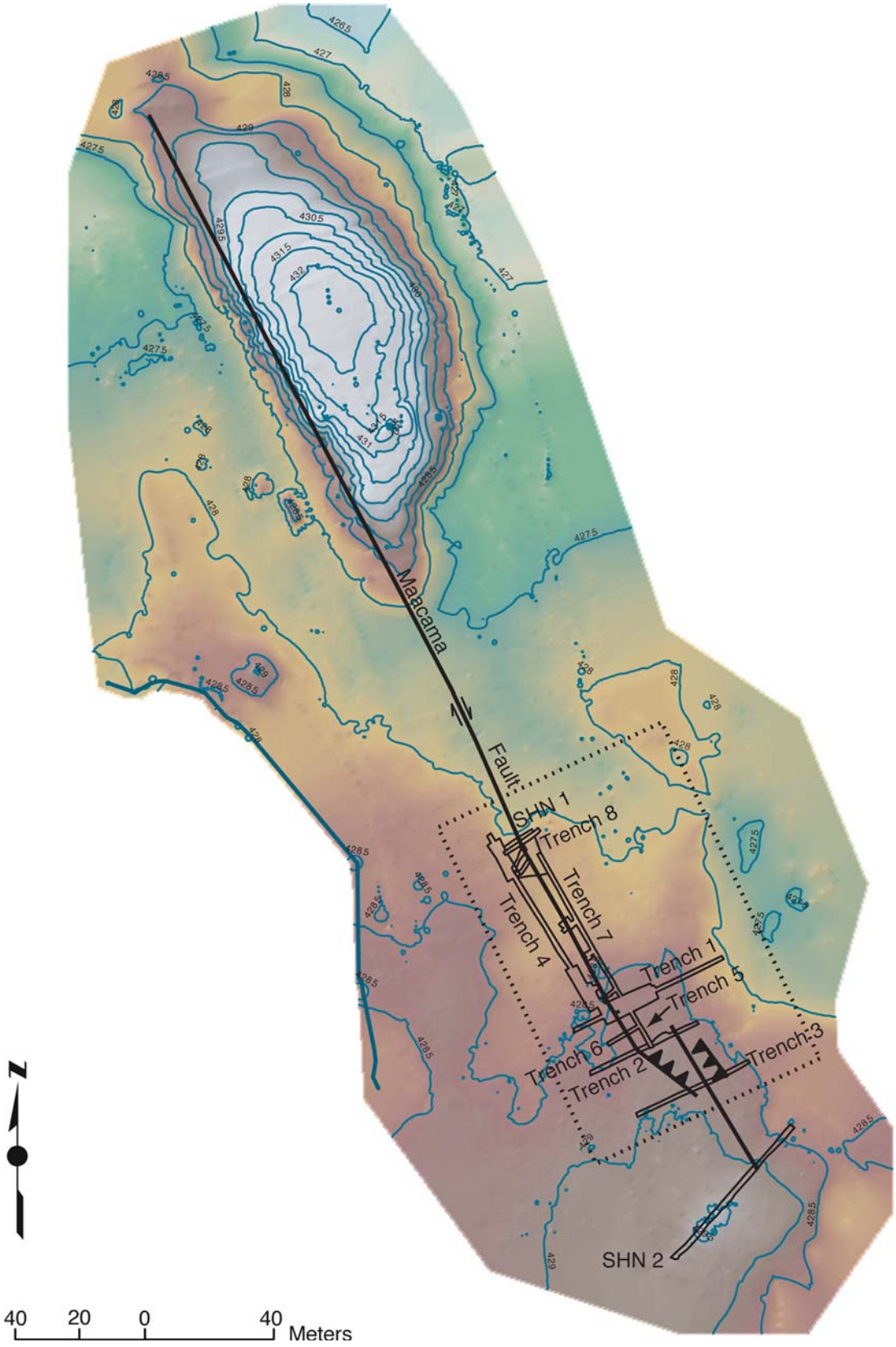

Figure 4. Detailed topographic map of the Haehl Creek site, derived from a kinematic Global Positioning System topographic survey. The contour interval is 0.5 m, and contour lines range in elevation from 426.5 to 432.5 m. Lighter shades indicate higher elevations. Heavy lines indicate Maacama fault traces; triangles indicate reverse faulting. The dashed rectangle shows the location of the area shown in Figure 5. The color version of this figure is available only in the electronic edition.

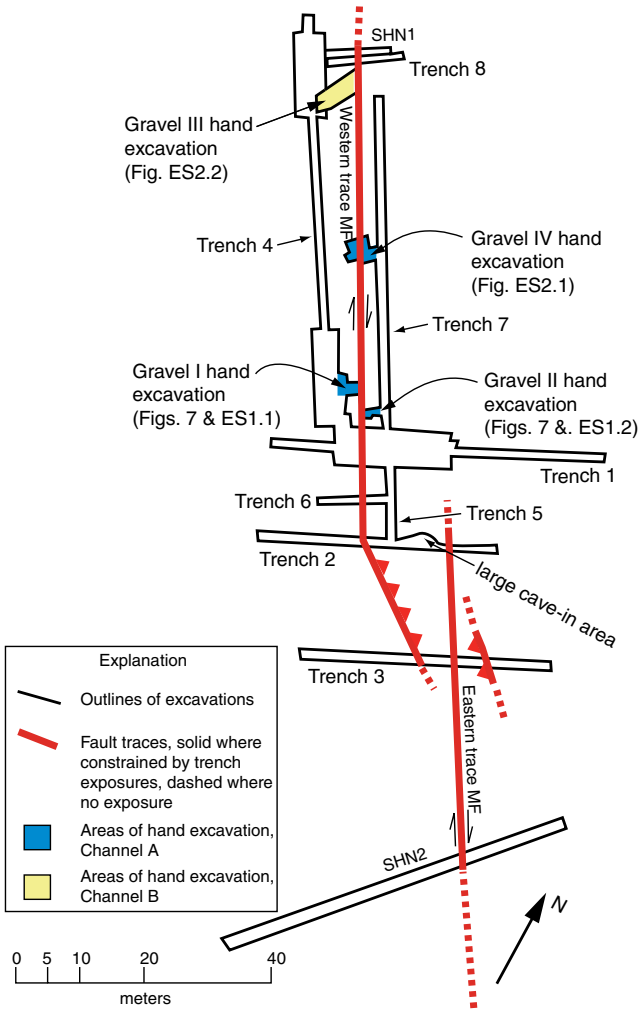

Figure 5. Detailed map showing fault zone and trenches. SHN1 and SHN2 are trenches excavated by SHN Consulting Engineers and Geologists, Inc. (SHN, 2004a,b) that provided the impetus for this research project. SHN2 provides a control for the location and nature of the fault zone southeast of our exposures. (MF, Maacama fault; triangles indicate upper plate of reverse faults.) The color version of this figure is available only in the electronic edition.

The remaining ages of samples collected from channel A fall into three age ranges. Seven samples fall into the 660–920 cal B.P. range and are indistinguishable within the error (group 2 in Table 1). Three samples fall into the 800–1170 cal B.P. range (group 3 in Table 1) and are also indistinguishable within the error. The remaining sample from channel A, sample 103, gives an age of 2360–2730 cal B.P. and is so far outside of the age ranges for the other 21 samples from channel A that we consider it to be anomalous and interpret it to be reworked (perhaps from channel B) or to be derived from near the center of an ancient redwood tree. We interpret these results to suggest that channel A was active some time during the interval between 1170 and 510 cal B.P. and subsequently abandoned about 500 years ago. The ages of eight additional samples collected from sediments that are stratigraphically older than channel A provide additional support for the young age of the channel (Table 1).

We collected four samples from channel B and two from adjacent sediments incised by channel B (Table 1). The four collected from channel B range from about 2500 to 3500 cal B.P. The youngest is sample 125, dated to 2490–2780 cal B.P., and we take this to most closely represent the age of this channel. The two samples collected from adjacent sediments into which channel B is incised give ranges of 3590–3830 and 3980–4230 cal B.P., consistent with the ages from channel B. The ages of samples collected from and adjacent to channel B are clearly distinct from those collected from channel A, with the sole exception of anomalous sample 103 from channel A. These relations show that channel B on the east side of the fault was cut away and replaced by channel A sediments and adjacent deposits.

Measurement of Channel Offset and Fault-Slip Rate

Fault-parallel trenches 4 and 7 provide the basis to constrain the right-lateral offset of the northern edge of channel A. We logged incremental slices (Figs. 7, Ⓔ S1, and S2), following the channel edge toward the fault. This method, though time consuming, allows the offset to be measured with a very small error estimate. We determined that the total offset of the northern margin of channel A is 4.6 ± 0.2 m. We could not measure the offset of the southern margin of channel A with similar precision because the southern margin east of the fault was inadvertently cut away in the area of the fault zone during excavation of trench 1. We note that the geometry of the gravel shows that the offset accumulated after the channel was abandoned. Had the channel flowed along the fault, we would have seen the margin turn and run parallel to the fault zone rather than heading directly into the fault. The modern channel of Haehl Creek is a good analog: no offset of the channel has accumulated even though the fault is actively creeping, because the fluvial processes are faster than the tectonic processes.

Our field interpretation was that gravel bodies III and IV were correlative and that we could measure the offset of channel B across the fault. We therefore excavated by hand and followed the channel edges to the fault in map view from trenches 4 and 7 (Ⓔ Figs. S3 and S4). However, radiocarbon analyses show that these two gravel bodies are of distinctly different ages and are not correlative. The offset equivalent of channel B on the eastern side of the fault must have been eroded sometime after 2500 cal B.P. (the best estimate for the age of channel B), otherwise this offset equivalent would have been exposed in the walls of fault-parallel trench 7 on the east side of the fault. Because we could not locate channel B east of the Maacama fault, it is not possible to determine the amount of offset of channel B. Accordingly, based on these exposures and radiocarbon ages, we interpret a meandering, offset channel A and a fault-truncated channel B (Fig. 10).

We calculate the fault-slip rate based on the offset of channel A and the youngest charcoal age from the channel

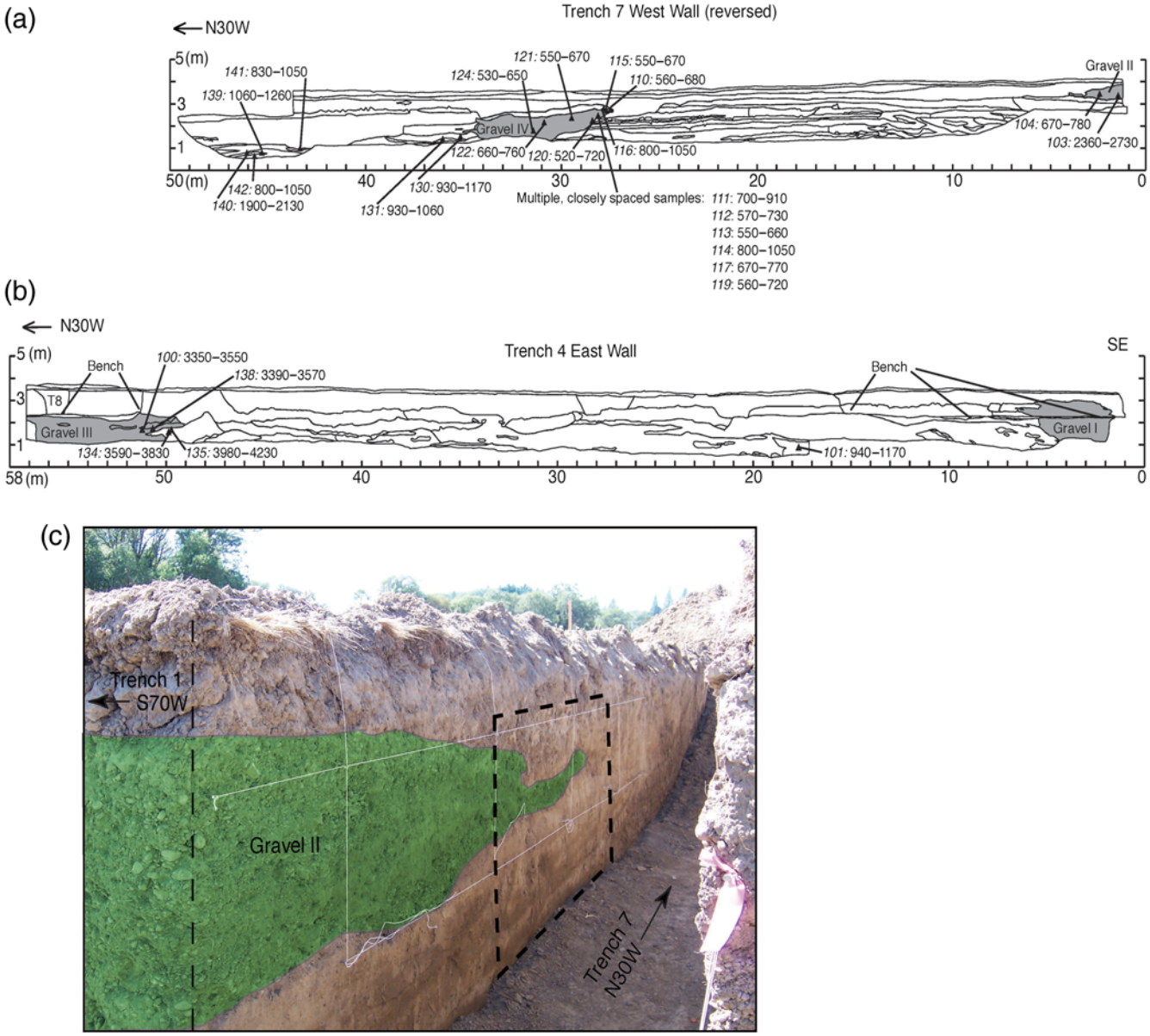

Figure 6. (a) The western wall of fault-parallel trench 7, east of the fault zone (log is reversed so the view is eastward) and (b) the eastern wall of fault-parallel trench 4, west of the fault zone. The shaded regions represent distinct gravel bodies, labeled gravel II (shown in c) and gravel IV in trench 7, and gravel I and gravel III in trench 4. Black triangles show the locations of radiocarbon samples (Table 1); sample numbers are in italic. The two-sigma age ranges are in calibrated years B.P. Ages associated with gravel III are significantly older than any of the ages from sediments in trench 7, indicating that the offset equivalent of gravel III was obliterated due to erosion. (c) The photo of the southeastern end of trench 7 shows the exposure of gravel II (shaded). The vertical dashed line on the left indicates the corner at the intersection of trenches 1 and 7. The heavy dashed rectangle shows the area where incremental sequential excavations exposed the northern edge of gravel II to determine its intersection with the fault zone. The string grid is 1 m horizontal by 0.5 m vertical. Ⓔ Detailed logs of these exposures can be found in the electronic supplement. The color version of this figure is available only in the electronic edition.

(sample 102, Table 1). Radiocarbon ages are given in years B.P., defined as years before 1950 C.E. Our offset measurement was made in 2004; and, because this is a creeping fault, part of the offset we measured has accumulated since 1950. Therefore, we adjust the age of sample 102 to years before 2000 C.E. by adding 50 years to the calibrated radiocarbon age range. This gives us our best estimate of the age of the offset, 560–690 years before 2000 C.E. The slip rate over the last 560–690 years is 6.4–8.6 mm/yr, derived from the youngest charcoal age for channel A (560–690 years before 2000 C.E.) and from the 4.6 ± 0.2 m offset determined by the incremental slice method. The channel A slip rate is larger than the historically measured creep rate, which is 5.7 ± 0.1 mm/yr over 20 years (McFarland *et al.*, 2013). Assuming the average creep rate has been constant over the last 560–690 years, the amount of strain not released as creep would be between 0.6 and 3.0 mm/yr. These measurements indicate that between 0.4 and 1.7 m of the total

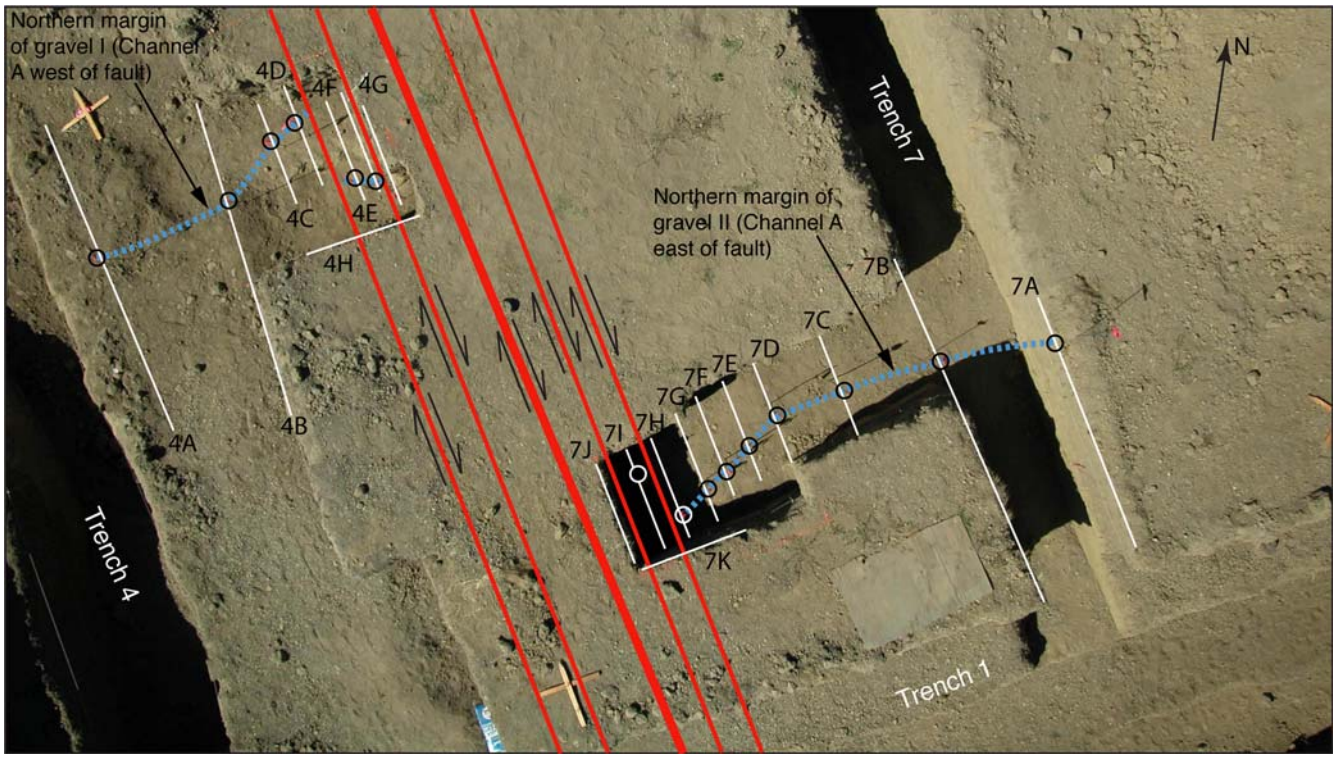

Figure 7. Kite aerial photo showing the zones of the incremental excavations to follow the northern edge of channel A (gravel bodies I and II) across the fault zone. Dashed lines indicate the northern edge of the channel; thin white lines show locations of each exposure logged. (Ⓔ For individual logs of each exposure see Figs. S1 and S2.) Circles show the locations of the northern channel edge in each exposure. The total offset between channel edge exposures 7H and 4D is 4.6 ± 0.2 m. The thickest line indicates the main fault trace, based on trench 1 exposure. Other heavy lines show locations of secondary faults related to smaller channel offsets. The distance between each logged slice varies from 20 cm to about 1 m. The color version of this figure is available only in the electronic edition.

offset of channel A could be due to coseismic slip, if the average creep rate has been constant since channel A was abandoned.

Prehistoric Surface Rupture

Most of our exposures did not provide evidence for individual earthquakes. In most exposures, the fault zone extended effectively to the ground surface or into massive, fine-grained units near the surface through which faulting was difficult or impossible to trace, consistent with a creeping fault (Hay *et al.*, 1989). However, in two exposures, trenches 2 and 6, we documented upward fault terminations that we interpret to be the result of coseismic slip during an earthquake. In trench 6, we exposed a zone of near-vertical strike-slip faults that offset a sequence of fluvial gravels and overlying fine-grained overbank deposits (Fig. 11). Three fault traces (A, B, and C in Fig. 11) terminate at the same horizon, offsetting units 60 and older, whereas the overlying units are offset only by the zone of faults farther west. We interpret these relations to indicate that an earthquake occurred after the deposition of unit 60 and before the deposition of unit 40. Subsequently, the faults to the west continued to move by creep, and possibly coseismically, as units 40–10 were deposited. We were unable to definitively determine how high in the section the western fault zone extends but were able to clearly document these faults disrupting units above the event horizon. We do not see additional evidence indicating surface rupture, such as fissure fills or scarp-derived colluvium (Lienkaemper *et al.*, 2002), that would strengthen the argument that these fault terminations are the result of an earthquake. We note that cessation of creep on these particular strands accompanied by a shift in the locus of creep to the more westerly strands could produce fault terminations such as these, a possibility that we cannot entirely rule out. However, we assume that the fault terminations represent a surface-rupturing earthquake, in part because (1) fault terminations do not occur in most of our fault-crossing trenches and (2) if a shift in fault creep to different strands has occurred, we would expect to see it reflected more widely throughout the exposures at this site.

Radiocarbon ages from units offset by faults A, B, and C show that this paleoearthquake occurred after the deposition of sample 105, with an age of 980–1260 cal B.P., and before deposition of sample 99, with an age of 740–920 cal B.P. (Table 2). These relations indicate that this earthquake occurred between 740 and 1260 cal B.P., assuming the radiocarbon ages are close to the age of deposition of the sedimentary units. We note that sample 98, from unit 30, also postdates the surface rupture and has an age of 690–910 cal B.P. (Table 2; Fig. 11), which is indistinguishable within the error from the age of sample 99. Because unit 30 is stratigraphically older

Table 1
Calculated Dates from Carbon-14 (^{14}C) Analysis of Charcoal Collected from Gravels and Associated Units Exposed in Haehl Creek Trenches

Group*	Sample Number	Gravel Unit (Trench)	Lab Number	δ^{13}C†	^{14}C Age (yr B.P.)‡	Calibrated Years B.P.§	Comments
Group 1	055	I (T1N)	AA66213‖	−21.3	590 ± 40	540–650	Channel A, group 1 (Ⓔ Fig. S5a)
Group 1	056	I (T1N)	193507#	−24.6	740 ± 50	560–760	Channel A, Group 1 (Ⓔ Fig. S5a)
Group 1	102	II (T7A)	AA66217‖	−24.6	530 ± 40	510–640	Youngest channel A, group 1, 560–690 yr before 2000 C.E. (Ⓔ Fig. S2)
Group 1	110	IV (T7)	AA66222‖	−23.0	670 ± 40	560–680	Channel A, group 1 (Fig. 6)
Group 1	112	IV (T7)	AA66224‖	−25.0	730 ± 40	570–730	Channel A, group 1 (Fig. 6)
Group 1	113	IV (T7)	AA66225‖	−26.5	620 ± 40	550–660	Channel A, group 1 (Fig. 6)
Group 1	115	IV (T7)	AA66227‖	−23.1	650 ± 40	550–670	Channel A, group 1 (Fig. 6)
Group 1	119	IV (T7)	AA66231‖	−23.2	700 ± 40	560–720	Channel A, group 1 (Fig. 6)
Group 1	120	IV (T7)	AA66774‖	−26.0	640 ± 80	520–720	Channel A, group 1 (Fig. 6)
Group 1	121	IV (T7)	WW5600**	—	650 ± 40	550–670	Channel A, group 1 (Fig. 6)
Group 1	124	IV (T7)	WW5602**	—	580 ± 40	530–650	Channel A, group 1 (Fig. 6)
Group 2	054	I (T1N)	AA66773‖	−26.2	830 ± 40	680–900	Channel A, group 2 (Ⓔ Fig. S5a)
Group 2	104	II (T7)	AA66219‖	−26.5	790 ± 40	670–780	Channel A, group 2 (Fig. 6)
Group 2	111	IV (T7)	AA66223‖	−25.4	870 ± 40	700–910	Channel A, group 2 (Fig. 6)
Group 2	117	IV (T7)	AA66229‖	−25.5	780 ± 40	670–770	Channel A, group 2 (Fig. 6)
Group 2	122	IV (T7)	WW5601**	—	770 ± 40	660–760	Channel A, group 2 (Fig. 6)
Group 2	144	I (T4H)	AA66236‖	−22.6	830 ± 40	680–900	Channel A, group 2 (Ⓔ Fig. S1)
Group 2	146	IV (T7J)	AA66754‖	−24.2	920 ± 40	740–920	Channel A, group 2 (Ⓔ Fig. S2)
Group 3	066	II (T1S)	193508§	−24.3	1120 ± 40	940–1170	Channel A, group 3 (Ⓔ Fig. S5b)
Group 3	114	IV (T7)	AA66226‖	−22.9	1010 ± 40	800–1050	Channel A, group 3 (Fig. 6)
Group 3	116	IV (T7)	AA66228‖	−24.9	1020 ± 40	800–1050	Channel A, group 3 (Fig. 6)
Pre-A	045	Adjacent to II (T1S)	WW5585**	—	850 ± 40	680–900	Predates upper channel A (Ⓔ Fig. S5b)
Pre-A	101	Below I (T4)	193933#	−23.3	1150 ± 40	940–1170	Predates channel A (Fig. 6)
Pre-A	103	II (T7)	AA66218‖	−24.6	2490 ± 50	2360–2730	Channel A, presumed to be reworked (Fig. 6)
Pre-A	130	Adjacent to IV (T7)	WW5603**	—	1110 ± 40	930–1170	Incised by channel A (Fig. 6)
Pre-A	131	Adjacent to IV (T7)	WW5604**	—	1080 ± 40	930–1060	Incised by channel A (Fig. 6)
Pre-A	139	Below IV (T7)	136438#	—	1220 ± 35	1060–1260	Predates channel A (Fig. 6)
Pre-A	140	Below IV (T7)	136439#	—	2055 ± 40	1900–2130	Predates channel A (Fig. 6)
Pre-A	141	Below IV (T7)	136440#	—	1035 ± 35	830–1050	Predates channel A (Fig. 6)
Pre-A	142	Below IV (T7)	136441#	—	1010 ± 35	800–1050	Predates channel A (Fig. 6)
Channel B	100	III (T4)	193932#	−25.2	3200 ± 40	3350–3550	Channel B (Fig. 6)
Channel B	125	III (T8)	AA66232‖	−23.2	2570 ± 50	2490–2780	Youngest channel B (Ⓔ Fig. S6b)
Channel B	127	III (T8)	AA66233‖	−22.0	3020 ± 40	3080–3340	Channel B (Ⓔ Fig. S6a)
Channel B	134	Adjacent to III (T4)	WW5597**	—	3440 ± 40	3590–3830	Incised by and interfingers with channel B (Fig. 6)
Channel B	135	Adjacent to III (T4)	WW5598**	—	3740 ± 40	3980–4230	Incised by and interfingers with channel B (Fig. 6)
Channel B	138	III (T4)	AA66234‖	−24.2	3260 ± 40	3390–3570	Channel B (Fig. 6)

*Group 1, 510–760 cal B.P.; group 2, 660–920 cal B.P.; group 3, 800–1170 cal B.P.; Pre-A, samples predating channel A.

†Δ^{13}C is assumed to be −25/00 if not reported.

‡Conventional radiocarbon age, expressed as years before 1950. Calculations assume a Libby half-life (5568 yr). Uncertainties are one standard deviation counting errors.

§Dendrochronologically calibrated, calendar age ranges using atmospheric decadal dataset of Reimer *et al.* (2009), two-sigma uncertainty, rounded to nearest decade. Calibration accomplished using CALIB (Stuiver and Reimer, 1993) revision 6.0 (see Data and Resources). B.P. is defined as before 1950.

‖Analyses from the National Science Foundation (NSF) Arizona Accelerator Mass Spectrometry Facility, University of Arizona, Tuscson, Arizona.

#Analyses from Beta Analytic Radiocarbon Dating Laboratory, Miami, Florida.

**Samples processed at the ^{14}C Laboratory of the U.S. Geological Survey, Reston, Virginia, and analyzed at the NSF Arizona Accelerator Mass Spectrometry Facility, University of Arizona, Tuscson, Arizona.

than unit 20, from which sample 99 was collected, the youngest 50 years of the age range of sample 98 (690–740 cal B.P.) cannot be included in the age range of unit 30, because the overlying unit 20 has an age range of 740–920 cal B.P. (based on the age of sample 99).

In trench 2, we documented two fault traces about 13 m apart: an eastern trace, which is a vertical strike-slip fault, and a western trace, which dips 48° to the northeast and is associated with a component of reverse slip and folding of overlying beds (Fig. 8 and Ⓔ S11). The eastern trace offsets

Table 2
Calculated Dates from ^{14}C Analysis of Charcoal Collected from Trenches 6 and 2 to Provide Age Constraints on Paleoearthquakes

Sample Number	Trench (Unit)*	Lab Number	$\delta^{13}C^{\dagger}$	^{14}C Age (yr B.P.)‡	Calibrated Years B.P.§	Comments
001	2S (unit 80)	WW5589$^{\|}$	—	1240 ± 40	1070–1270	Postfault, eastern trace
002	2S (unit 100)	WW5590$^{\|}$	—	1450 ± 40	1300–1400	Prefault, eastern trace
004	2S (unit 90)	WW5592$^{\|}$	—	1140 ± 40	960–1170	Prefault, eastern trace
005	*2S (unit 70)*	*WW5593*$^{\|}$	—	*2170 ± 40*	*2060–2320*	Reversed
006	*2S (unit 70)*	*WW5594*$^{\|}$	—	*1350 ± 40*	*1180–1340*	*Reversed*
007	2N (unit 80)	WW5586$^{\|}$	—	1230 ± 40	1060–1270	Postfault, eastern trace
009	2S (unit 90)	141952$^{\#}$	—	1155 ± 35	980–1170	Prefault, western trace
010	2S (110)	WW5595$^{\|}$	—	1100 ± 40	930–1120	Prefault, western trace
012	2N (unit 95)	WW5587$^{\|}$	—	1300 ± 40	1140–1300	Prefault, eastern trace
013	2N (unit 95)	WW5588$^{\|}$	—	1160 ± 40	970–1180	Prefault, eastern trace
015	2N (unit 70)	141953$^{\#}$	—	1195 ± 35	1000–1260	Postfault prefold; western trace
015R		141963$^{\#}$		1180 ± 35	980–1230	
016	2N (unit 70)	141954$^{\#}$	—	1210 ± 35	1060–1260	Postfault prefold; western trace
017	*2N (unit 70)*	*141955*$^{\#}$	—	*1495 ± 44*	*1300–1520*	Reversed
018	2N (unit 60)	141956$^{\#}$	—	1060 ± 35	930–1060	Postfault prefold; western trace
19	*2N (unit 80)*	*141957*$^{\#}$	—	*1750 ± 35*	*1560–1780*	*Reversed*
020	2S (unit 80)	141958$^{\#}$	—	1115 ± 35	930–1170	Postfault prefold; western trace
021	2N (unit 50)	141959$^{\#}$	—	1050 ± 35	920–1060	Postfold (?); western trace
022	2N (unit 40)	141960$^{\#}$	—	960 ± 35	790–930	Postfold; western trace
022R		141964$^{\#}$		975 ± 30	800–940	
46	2N (unit 100)	141961$^{\#}$	—	1065 ± 55	800–1170	Prefault; western trace
092	2N (unit 40)	141962$^{\#}$	—	1080 ± 30	930–1060	Postfold
093	6N (unit 60)	AA66214**	−25.2	1260 ± 40	1080–1280	Prefaulting event
096	6N (unit 60)	AA66215**	−25.8	1250 ± 40	1080–1280	Prefaulting event
098	6N (unit 30)	AA66216**	−25.8	860 ± 40	690–910	Postfaulting event
099	6N (unit 20)	AA66755**	−23.4	920 ± 40	740–920	Postfaulting event
105	6N (unit 60)	AA66772**	−25.3	1190 ± 60	980–1260	Prefaulting event
108	6N (unit 60)	WW5599**		1220 ± 40	1060–1270	Pre–event
109	*6N (unit 30)*	*AA66221*	−25.3	*2100 ± 40*	*1950–2300*	*Reversed*

Italic print indicates sample is stratigraphically reversed.

*See Figure 11 for trench 2 sample locations; see Figure 10 for trench 6 sample locations.

$^{\dagger}\Delta^{13}C$ assumed to be −25/00 if not reported.

‡Conventional radiocarbon age, expressed as years before 1950. Calculations assume a Libby half-life (5568 yr). Uncertainties are 1 standard deviation counting errors.

§Dendrochronologically calibrated, calendar age ranges using atmospheric decadal dataset of Reimer *et al.* (2009), two-sigma uncertainty, rounded to nearest decade. Calibration accomplished using CALIB (Stuiver and Reimer, 1993) revision 6.0 (Data and Resources Section). B.P. is defined as before 1950.

$^{\|}$Samples processed at the ^{14}C Laboratory of the U.S. Geological Survey, Reston, Virginia, and analysed at the NSF Arizona Accelerator Mass Spectrometry Facility, University of Arizona, Tuscson, Arizona.

$^{\#}$Analyses from Lawrence Livermore Laboratory, Livermore, California. R in sample number denotes repeat measurement.

**Analyses from NSF Arizona Accelerator Mass Spectrometry Facility, University of Arizona, Tuscson, Arizona.

alluvial deposits no older than 1180 cal B.P. (sample 13, Table 2). Unfaulted sediment deposited over the truncated fault is no younger than 1060 cal B.P. (sample 7, Table 2), assuming the radiocarbon ages are close to the time of deposition of the sedimentary units. Therefore, based on these relations, the most recent earthquake exposed in trench 2 has an age constrained to 1060–1180 cal B.P. We interpret the event horizon in trenches 2 and 6 to be the same earthquake because the calibrated age ranges are indistinguishable within the error. If this is correct, this earthquake occurred 1060–1180 cal B.P. (770–890 C.E.) because the constraining age interval for the earthquake exposed in trench 2 (1060–1180 cal B.P.) is contained within the constraining age interval for the earthquake exposed in trench 6 (740–1260 cal B.P.). We refer to this event as the Willits surface rupture and plot its age range on the *x* axis of Figure 12. No subsequent fault slip, either coseismic or creep, has occurred on the eastern trace exposed in trench 2 (Fig. 8). In trench 6, subsequent creep (with or without coseismic slip) has occurred on the fault strands west of faults A, B, and C (Fig. 11).

The western fault trace exposed in trench 2 most likely records the same earthquake, expressed by an eroded fault scarp that was buried by the deposition of unit 80. This fault trace is the on-strike projection of the western fault exposed in trench 6 (Fig. 11). The surface rupture, as recorded on the eastern trace of trench 2, occurred before the deposition of unit 80, because that unit is unfaulted (Fig. 8). Unit 80 is also the oldest unit that crosses the western fault with no brittle offset (Fig. 8). Units older than 80 in the hanging wall of the western trace exposed on the northern wall of trench 2 (units

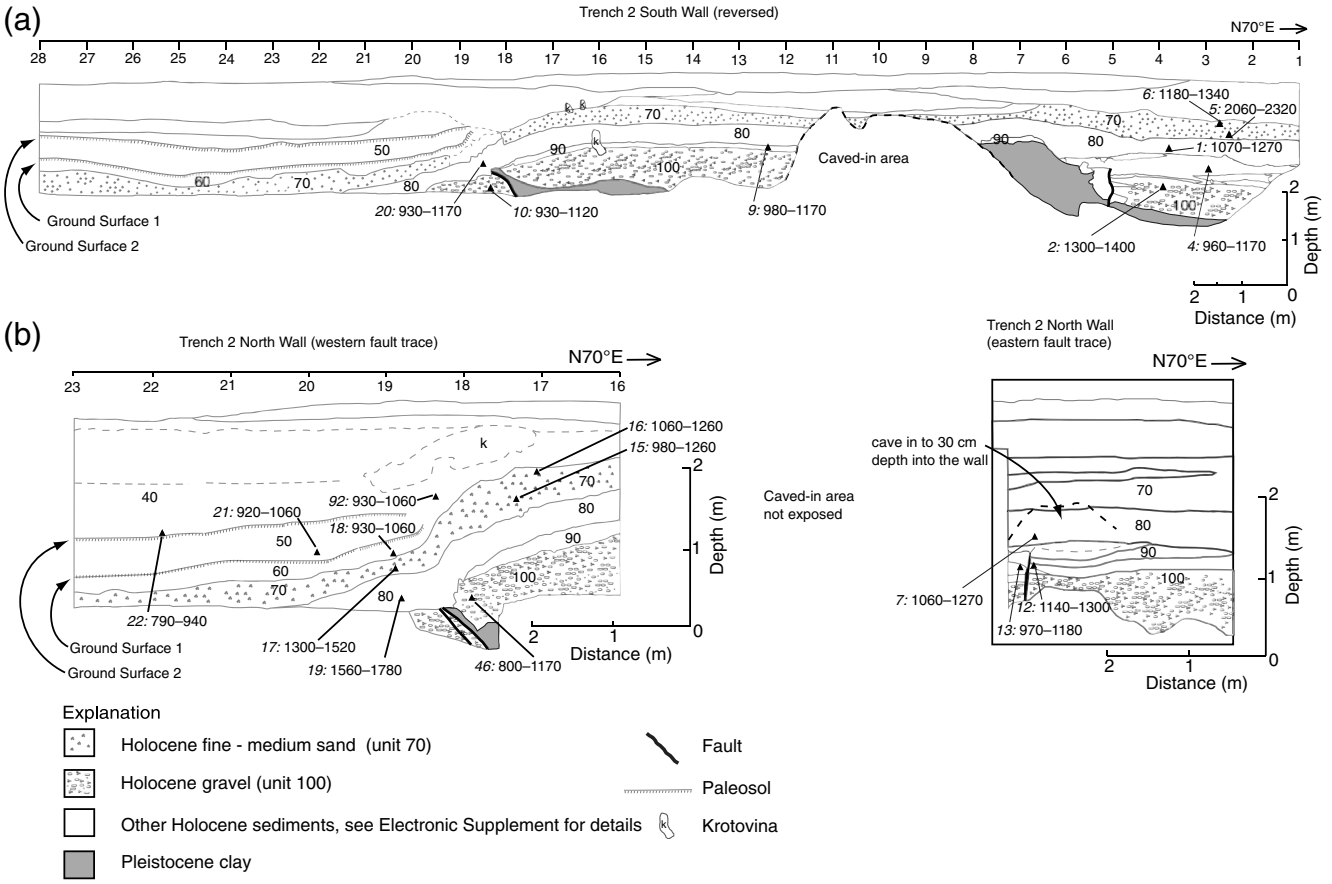

Figure 8. (a) The southern wall of trench 2 (log is reversed so view is northward), and (b) the northern wall of trench 2. Black triangles show the locations of radiocarbon samples (Table 2); sample numbers are in italic. Ages are in calibrated years B.P., with two-sigma age ranges. (left) The western fault. Units 90–100 were deposited before an earthquake that formed the scarp that truncates these units. Units 80, 70, and 60 (up to and including ground surface 1) were folded some time after the scarp formed. Ground surface 2 is not folded. (right) The eastern fault. Units 90 and below are faulted; unit 80 is not. Fault slip is bracketed by samples 7 and 13 and occurred between 1060 and 1180 cal B.P.

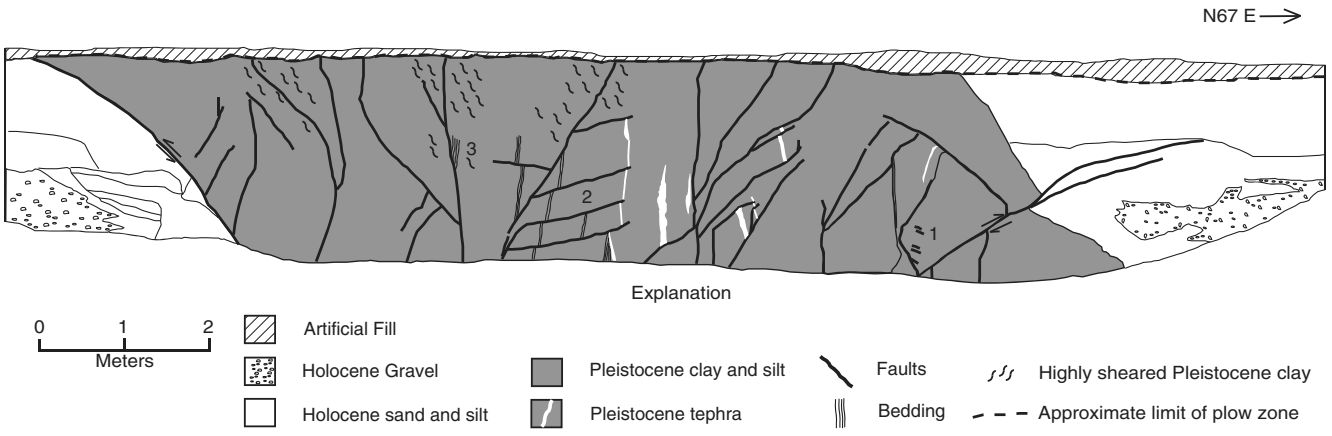

Figure 9. Part of the trench 3 log south wall (reversed so the view is northward) showing faults in the stepover region. The western fault trace, which is a reverse fault in trench 3, is on strike with the subvertical fault zone that is exposed in trench 6 (Fig. 11) and trench 1 (Ⓔ Fig. S5). The easternmost fault, a thrust fault, is not observed in other fault-perpendicular trenches. One or several of the subvertical faults exposed in trench 3 connect along strike to the south to the vertical fault zone exposed in SHN2 trench (Fig. 5) and to the north connects to the eastern fault trace exposed in trench 2. Measurements of bedding attitudes within the Plesistocene units taken at locations 1, 2, and 3, are N53°W, 86° SW; N57°W, 85° SW; and N53°W, 86° SW, respectively. The Ⓔ full log of this exposure is included in Figure S7 of the electronic supplement.

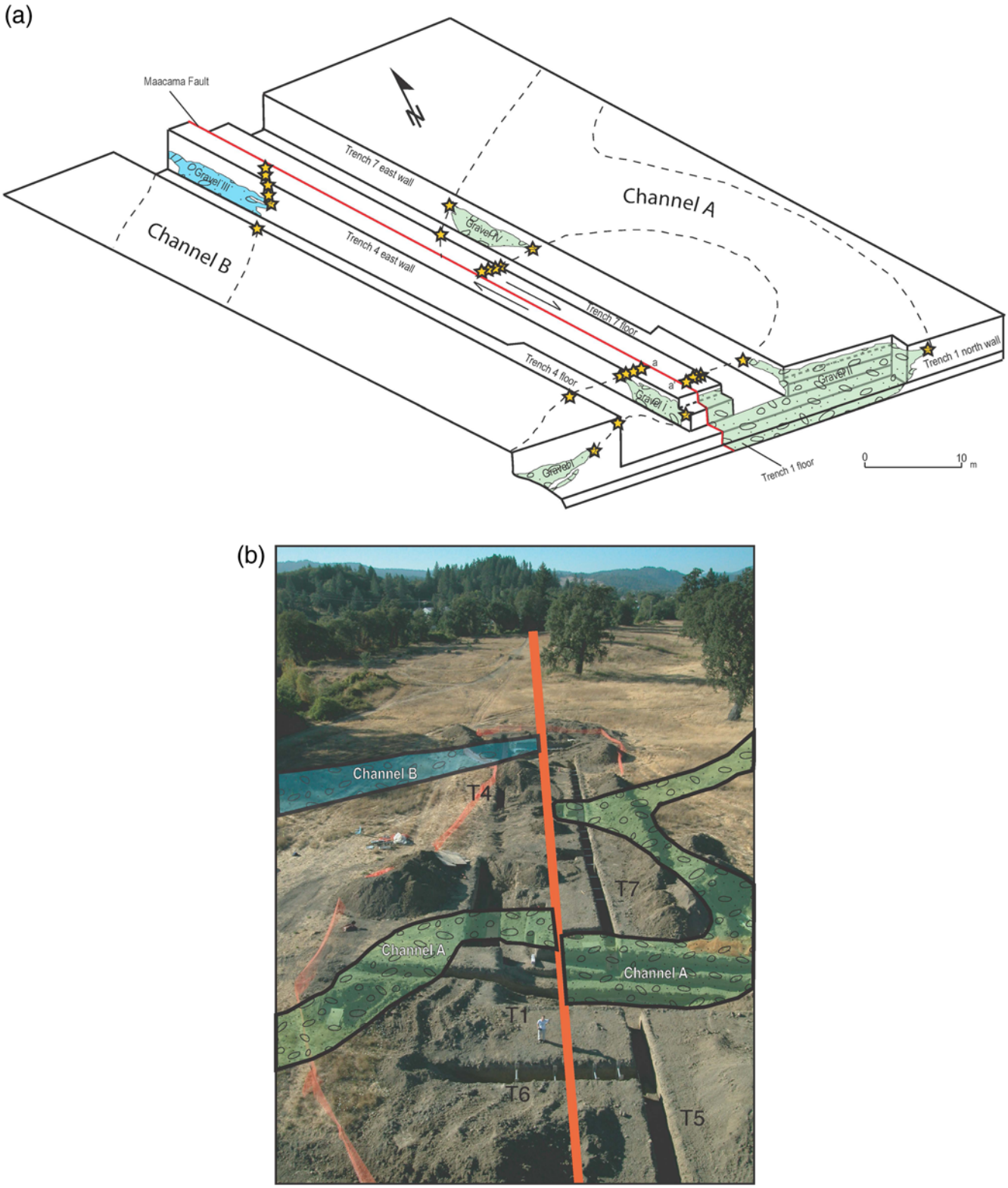

Figure 10. (a) Block diagram of trenches 1, 4, and 7 showing exposures of the gravel units comprising channels A and B. Stars mark the exposures of the channel edges; overlapping stars show areas where channel edges were traced to the fault, either continuously in map view or incrementally using vertical slices. The distance from a to a' (offset of the northern edge of channel A) is 4.6 ± 0.2 m. (b) Kite aerial photograph with our interpretation of channel geometries superimposed. The heavy line represents the Maacama fault zone. The color version of this figure is available only in the electronic edition.

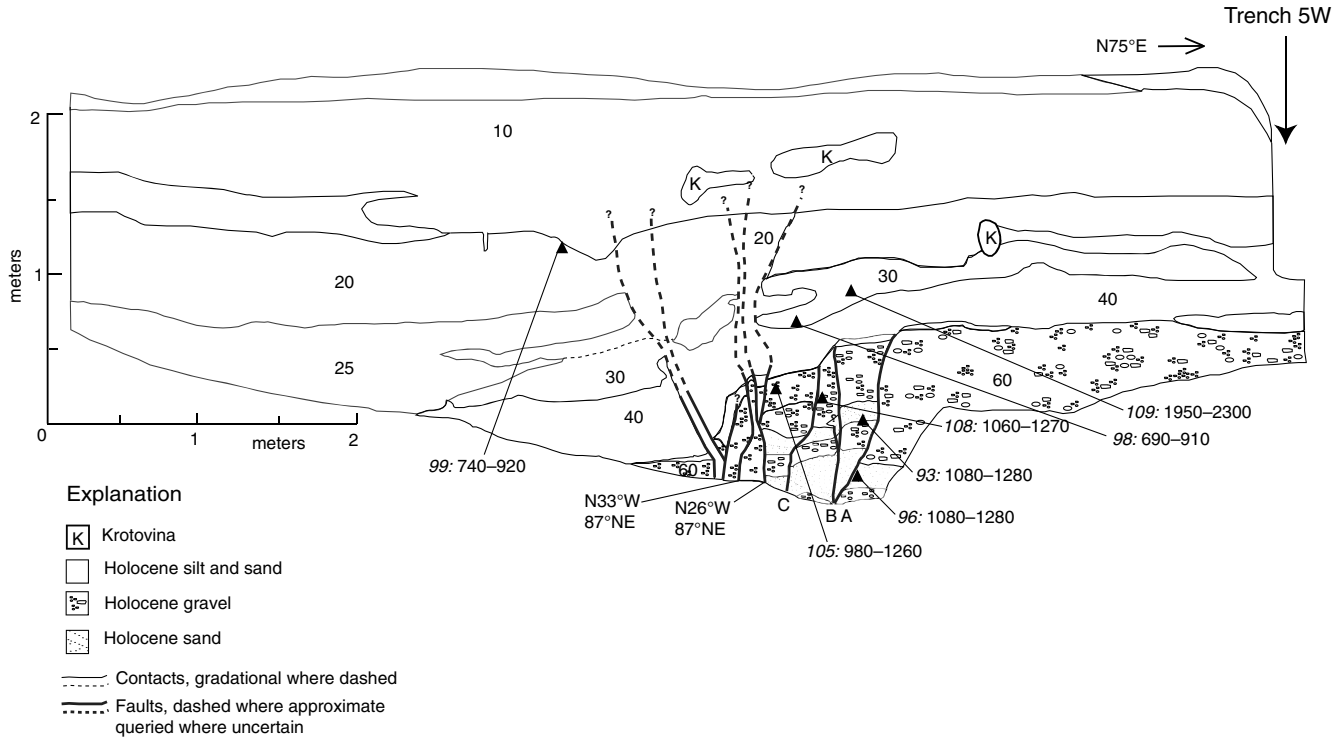

Figure 11. Log of the fault zone exposed in trench 6, south wall (reversed so the view is northward). Black triangles show the locations of radiocarbon samples (Table 2); sample numbers are in italic. Ages are in calibrated years B.P., with two-sigma age ranges. Three faults (labeled A, B, and C) terminate below unit 40. Western faults break units 40 and above and can be traced nearly to the ground surface. We interpret these relations to indicate a surface-rupturing earthquake occurred before the deposition of Unit 40. The age of fault slip for faults A, B, and C is bracketed by samples 105 and 99 and occurred between 740 and 1260 cal B.P.

90 and 100, Fig. 8) appear to be eroded and do not extend across the fault. This likely represents an eroded fault scarp that was buried by the deposition of unit 80, and we interpret these relations to indicate that the western trace also records a surface-rupturing event at the same time as the eastern fault trace. Samples 10 and 46 predate this earthquake (Fig. 8) and have age ranges of 930–1120 and 800–1170 cal B.P., respectively (Table 2), consistent with the age range determined for this earthquake based on the termination of the eastern fault and the terminations exposed in trench 6. Sample 16 (1060–1260 cal B.P.) postdates this faulting event, which is also consistent with the age of the earthquake established on the eastern trace and in trench 6. This earthquake may also be recorded in trench 3, where the easternmost fault trace terminates below a unit containing sample 75, which has an age range of 920–1050 cal B.P. (Ⓔ electronic supplement part 3). The underlying faulted unit contains sample 72, which has an age range of 1550–1770 cal B.P. However, we have very little age control for this event in trench 3; and, while the ages allow this fault termination to be related to the Willits surface rupture, the relations in trench 3 do not provide any additional constraints on its age.

Fault Stepover and Late Holocene Folding Event

Fault perpendicular trenches 1, 6, 2, and 3 (north to south, Fig. 5) document that the Maacama fault steps left from one trace to another over an along-strike distance of about 60 m. The stepover zone, which is about 15 m wide, is a zone of compression, as demonstrated by reverse faults exposed in trenches 2 and 3 (Figs. 8, 9, and Ⓔ electronic supplement part 4), by a monoclinal fold developed in the late Holocene sediments overlying the western fault trace exposed in trench 2 (Fig. 8) and by the near-vertical Pleistocene beds between the two major faults exposed in trench 3 (Figs. 9 and Ⓔ S12). The near-vertical Pleistocene beds exposed in trench 3 show that this compression has been active over the long term, indicating that the stepover is a persistent feature of the fault zone at this location. Between trenches 6 and 2, which are only 5 m apart, the character of the fault zone and associated deformation change radically from a typical subvertical strike-slip fault zone in trench 6 (Fig. 11) to two distinct fault zones 13 m apart in trench 2 (Figs. 8). The western trace is on strike with the fault zone exposed in trench 6 (Fig. 11) and trench 1 (Ⓔ Fig. S5), but in trench 2 the fault is dipping and is associated with oblique reverse displacement and folding of Holocene units (Figs. 8 and Ⓔ S11). The eastern trace exposed in trench 2, in contrast, is a vertical strike-slip fault with no associated folding (Fig. 8) and does not appear in any trench north of trench 2 (Fig. 5). However, folded beds near the bottom of trench 1 at the eastern end (trench 1, meters 8–16; Ⓔ Fig. S5) could represent the northernmost expression of deformation associated

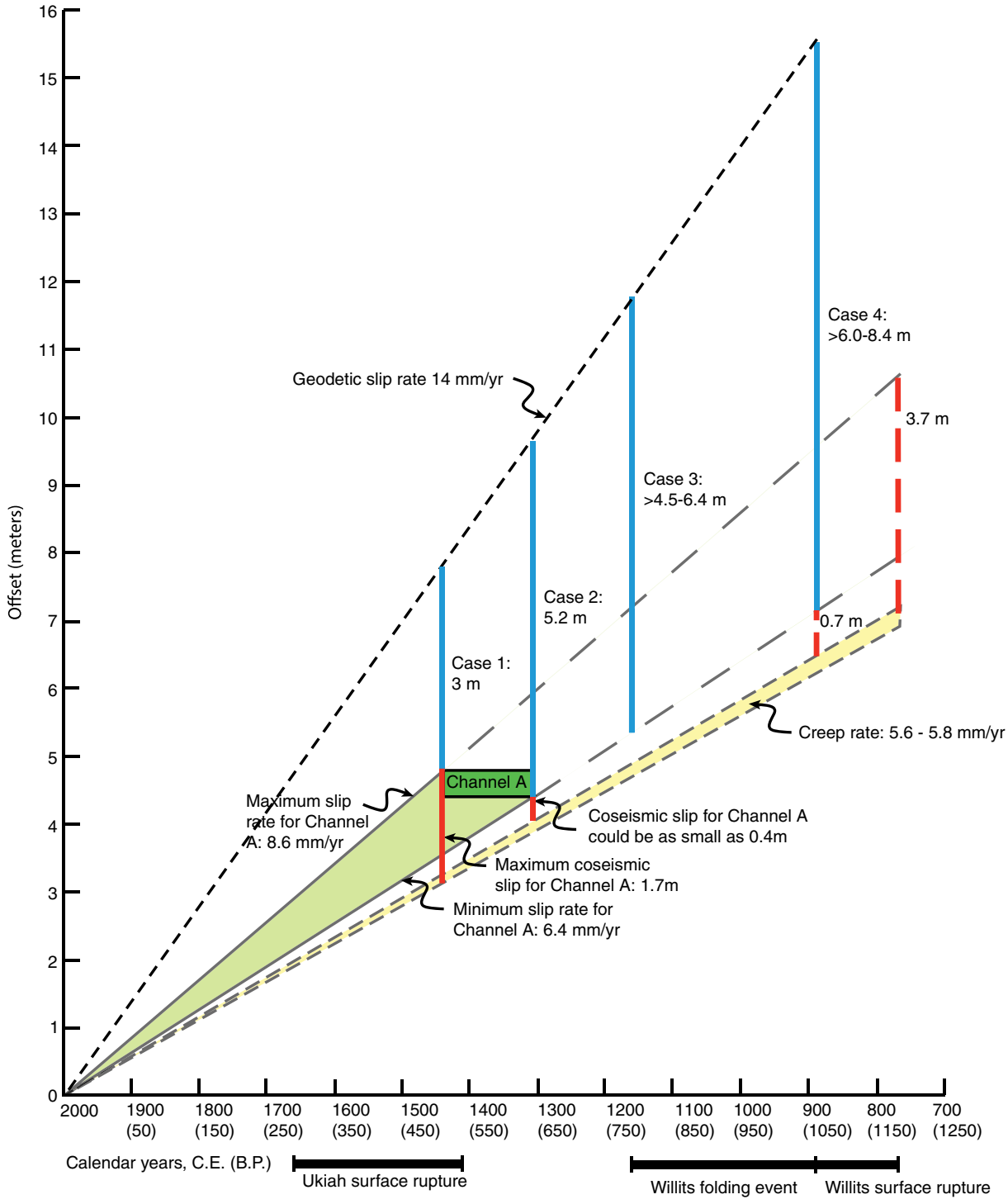

Figure 12. Displacement occurring over time shows the surface creep rate, the geologic slip rate based on the offset of channel A, and the geodetically modeled slip rate. The age constraints for the Willits surface rupture, Willits folding event, and Ukiah surface rupture are shown along the *x* axis, and the age and offset constraints for channel A are plotted. Channel A is offset more than expected if the average creep rate has been constant, implying either coseismic offset in addition to creep or a higher creep rate in the past. If channel A has been offset coseismically and the average creep rate has been constant, then the coseismic slip for channel A is 0.4–1.7 m, and age constraints allow this to be due to the Ukiah surface rupture. If the geodetically modeled slip rate of 14 mm/yr reflects the true long-term slip rate across the fault zone, this implies a significant slip deficit in light of the slip rate derived from the age and offset of channel A. Given the age range of channel A, the slip deficit would be 3 m (case 1) to 5.2 m (case 2). In case 3, no large earthquake has occurred at this site after the folding event recognized in trench 2, implying a slip deficit of 4.5–6.4 m. In case 4, the most recent large earthquake is the faulting event recognized in trenches 2 and 6, implying a slip deficit of 6–8.4 m. Alternatively, if the geologic slip rate is considered instead of the geodetic rate and only creep at the modern rate has occurred since the Willits surface rupture 1060–1180 cal B.P., then the slip deficit would be 0.7–3.7 m (heavy dashed lines). The color version of this figure is available only in the electronic edition.

with the eastern fault as it dies out along strike to the north. Southeast of trench 2, the eastern trace is part of the wide zone of oblique reverse faulting exposed in trench 3 (Fig. 9) and is a narrow, subvertical, strike-slip fault zone exposed in SHN2 (Fig. 5; SHN, 2004a,b).

Folded and faulted Pleistocene beds at or near the ground surface characterize the compressional zone associated with the stepover (Fig. 9 and Ⓔ S12). Southeast of trench 2, about 17 m along strike of the fault, Pleistocene lacustrine units are exposed at the ground surface in trench 3 and are thrust over Holocene alluvial deposits on both eastern and western faults (Fig. 9). The well-bedded Pleistocene section exposed in trench 3 is near vertical, and slickensides along the western fault trace indicate oblique reverse faulting (Ⓔ Fig. S7). South of trench 3, all slip is transferred to the steeply dipping strike-slip fault zone exposed in the southern SHN trench (SHN, 2004a,b). No deformation of units outside of this single fault zone appears in this SHN trench.

In trench 2, the eastern fault trace records an earthquake associated with surface fault rupture between 1060 and 1180 cal B.P. (770–890 C.E.), as discussed above (Fig. 8). There is no deformation of the sediments overlying the event horizon near this fault, indicating that the eastern fault trace is not creeping at the latitude of trench 2 and has not ruptured in any subsequent earthquakes. In contrast, the units overlying the western trace have been deformed by compression and therefore may record a younger earthquake. In trench 2, units 80, 70, and 60 are folded into a westerly-facing monocline in which the axis is coincident with the western fault trace (Figs. 8 and Ⓔ S11). This fold formed either in response to ongoing creep or during a later coseismic event that was not accompanied by brittle surface rupture on either fault trace exposed in trench 2. Our analysis, based on two lines of evidence, suggests the fold formed in response to a rapid deformation event. First, all units exposed in trench 2 east of the fold axis are dipping the same amount (about 20°), including units above and below the event horizon of the 1060–1180 cal B.P. earthquake (Fig. 8). If the fold had formed as the result of slow, constant creep, younger units would be tilted progressively less than older units. Second, we mapped two paleo-ground surfaces within unit 60 west of the monocline axis, labeled ground surface 1 and ground surface 2 in Figure 8. Ground surface 1 is dipping the same amount as underlying units 70 and 80 (about 20° at meter 19, and about 60° at meter 18.5), whereas ground surface 2 does not appear to be folded. We interpret this to indicate that the folding occurred while ground surface 1 was the active ground surface and that no deformation has occurred since this time. Unit 40 thickens west of the fold axis, suggesting that this unit filled in the low area created by the monocline. If this analysis is correct, an earthquake that caused folding, but not brittle faulting within the fault stepover, occurred after the 1060–1180 cal B.P. event. Samples 9, 15, 16, 18, and 20 predate the folding and indicate that the folding occurred sometime after 1060 cal B.P. (Table 2; Fig. 8). Sample 22 postdates the folding, indicating the folding occurred prior to 790 cal B.P. (Table 2; Fig. 10). Subsequent to this folding event, which occurred between 790–1060 cal B.P. (890–1160 C.E.), neither fault exposed in trench 2 appears to record any creep or any coseismic displacement. We hypothesize that the compressional stepover inhibits fault creep and that deformation within the stepover only occurs coseismically. We refer to this event as the Willits folding event and plot its age range on the *x* axis of Figure 12.

Units 20 through 40 exposed in trench 6 also appear to be folded across the fault zone (Fig. 11). These units postdate the surface rupture, and the folding could have occurred during the folding event associated with the western trace exposed in trench 2. However, the trench 6 exposure lacks any definitive evidence showing whether the geometry of these units is due to ongoing fault creep or to a distinct folding event.

The western fault trace in trench 2 is a dipping fault; folding would have modified its dip. Because the folding occurred after the most recent surface-faulting event recorded on the western fault in trench 2, subsequent folding would have increased the near-surface dip of the fault. If the dip of the overlying units is removed, the 48° dip of the fault would be restored to an initial steeper dip of 68°.

Discussion

Slip Rate at Haehl Creek and Earthquake History of Ukiah and Willits Areas

The slip rate derived from offset channel A, 6.4–8.6 mm/yr over the last 560–690 years (before 2000 C.E.), is higher than the historically measured 5.7 ± 0.1 mm/yr average creep rate (Fig. 12). Therefore, either the creep rate over the last 560–690 years has been faster than the average over the last 20 years or the channel A offset is the result of creep plus coseismic displacement. If part of the offset is due to a large earthquake, the coseismic offset is 0.4–1.7 m, assuming the average creep rate determined over the last 20 years is constant over the time interval since channel A was abandoned (Fig. 12).

Based on the upward truncations of fault strands exposed in trenches 2 and 6, and based on the buried, eroded scarp in trench 2, we interpret that an earthquake produced coseismic ground rupture prior to the deposition of channel A gravels, between 1060 and 1180 cal B.P. (770–890 C.E.; Fig. 12, Willits surface rupture). On the eastern fault trace exposed in trench 2, the Willits surface rupture is the most recent deformation of any kind. On the western trace exposed in trench 6, creep with or without one or more subsequent earthquakes occurred. On the western trace exposed in trench 2, a monocline developed between 790 and 1060 cal B.P. (890–1160 C.E.; Fig. 12, Willits folding event), but no younger deformation has occurred.

This evidence shows that the Maacama fault is capable of producing infrequent earthquakes large enough to produce surface rupture and folding in the Willits area. This is consistent with the results from a paleoseismic study in Ukiah, 25 km southeast of the Haehl Creek site (Sickler *et al.*, 2005). At the West Fork site in Ukiah, a prehistoric surface rupture

occurred between 290 and 540 cal B.P. (1410–1660 C.E.; Sickler *et al.*, 2005; Fig. 12, Ukiah surface rupture). It is possible that the fault rupture associated with this event propagated through Willits and caused up to 1.7 m of coseismic displacement of channel A at the Haehl Creek site. If fault rupture associated with this earthquake did occur at this site, it is not recorded as a paleoearthquake distinct from creep in any of the Haehl Creek trenches, though a surface rupture could have occurred on any of the creeping traces exposed in trenches 1, 3, 6, and 8. Neither fault exposed in trench 2 shows any evidence for slip post-channel A time. However, because of the cave-in that occurred between the eastern and western fault traces documented in trench 2, we cannot rule out a fault zone in between these traces that could have slipped during the Ukiah paleoearthquake.

Geodetically Determined Far-Field Slip Rates: Implications for a Slip Deficit

The $13.9(+4.1/-2.8)$ mm/yr geodetically-derived far-field displacement rate for the Maacama fault (Freymueller *et al.*, 1999) is significantly higher than our calculated slip rate of 6.4–8.6 mm/yr over the last 560–690 years (Fig. 12). Whether our slip rate is due entirely to creep or to creep plus an earthquake, if the geodetic rate is representative of the long-term strain accumulation rate across the Maacama fault, there is a significant slip deficit accumulated since the abandonment of channel A. Figure 12 illustrates that the slip deficit would be 3 m if channel A is 560 years old (case 1) and 5.2 m if channel A is 690 years old (case 2). We note that a future earthquake involving at least 3 m of slip would largely eliminate the discrepancy between the geologic and geodetic rates, and this illustrates the importance of considering the earthquake cycle when calculating geologic slip rates (M. Rizza *et al.*, unpublished manuscript, 2014).

The slip deficit between the geodetic and geologic slip rates becomes even greater if we consider the possibility that the most recent large earthquake is the Willits folding event that occurred before 1160 C.E. If the geologic slip rate of 6.4–8.6 mm/yr reflects the long-term creep rate (i.e., the creep rate has been faster than the average rate measured over the last 20 years), then the slip accumulated across the fault in that time would be at least 4.5–6.4 m (case 3, Fig. 12). The deficit is greater still if the folding was not coseismic, and the most recent large earthquake is the Willits surface rupture that occurred 770–890 C.E. In this scenario, the difference between the geodetic and geologic slip rates would imply at least 6.0–8.4 m of accumulated slip (case 4, Fig. 12).

Several alternate conclusions can be drawn from this analysis. (1) The Maacama fault is due for a large earthquake, involving at least 3 m of horizontal fault slip. (2) There are other parallel fault traces that accommodate the excess slip. (3) The geodetic slip rate does not reflect the long-term geologic slip rate. The first scenario, an earthquake involving at least 3 m of horizontal fault slip, implies the fault is due for an earthquake of approximately **M** 7.5 (Wells and Coppersmith, 1994).

It is possible that other faults subparallel to the Maacama fault may accommodate some part of the slip deficit between the geodetically modeled slip rate and the geologic slip rate (scenario 2). A Quaternary fault, here referred to informally as the East Willits fault, bounds the eastern edge of the Little Lake Valley (Upp, 1989; Woolace, 2005; Erickson, 2008). The trace of the East Willits fault overlies the most pronounced gravity anomaly (up to 12 mGal) in Little Lake Valley (Erickson, 2008). Based on analysis of stratigraphy from well logs, Woolace (2005) inferred that an up-to-the-east, subvertical fault bounding the eastern edge of the Little Lake Valley juxtaposes late Quaternary basin fill against Mesozoic Franciscan bedrock. Our analysis of recently acquired EarthScope Light Detection and Ranging (LiDAR) data reveals landforms suggestive of possible Holocene slip on at least a 4 km long section of the East Willits fault (Fig. 13). More work aimed at identifying other Holocene faults is needed to test scenario 2, especially using new techniques such as LiDAR to image areas beneath the forest canopy. We suggest that paleoseismic study of the East Willits fault could help to determine whether or not it has accommodated Holocene slip.

If the geodetically modeled slip rate does not reflect the long-term geologic slip rate, the slip deficit is much lower, assuming the average creep rate has been constant. If the channel A slip rate (6.4–8.6 mm/yr) reflects the long-term slip rate and the long-term average creep rate is 5.6–5.8 mm/yr, then 0.6–3 mm/yr of strain accumulates across the fault. If the most recent earthquake to release all accumulated strain is the Willits surface rupture recorded in our trenches 1060–1180 cal B.P., then the current strain accumulated is 0.7–3.7 m (Fig. 12); and, if the Ukiah surface rupture (1410–1660 C.E.) involved surface rupture in Willits that released all accumulated strain, then the slip deficit today is 0.2–1.8 m.

Conclusions

The right-lateral Maacama fault in Willits, California, one of three major strike-slip faults that define the transform plate boundary at this latitude, is a creeping fault that also appears to produce infrequent, large earthquakes. Our results suggest that fault creep is impeded within the local restraining stepover that we document at the site. If this behavior is typical of creeping faults, future paleoseismic sites on creeping faults may be more successful in exposing evidence for earthquakes if they are sited within stepovers. The slip rate documented at this site over the last 560–690 years is 6.4–8.6 mm/yr, somewhat higher than the historic average creep rate of 5.7 ± 0.1 mm/yr. Based on both our measured slip rate at the Haehl Creek site and on evidence that we interpret to represent prehistoric earthquakes in 1060–1180 cal B.P. (770–890 C.E.) and 790–1060 cal B.P. (890–1150 C.E.), we infer that the Maacama fault produces large infrequent earthquakes. If coseismic slip has occurred in the last 690 years at Haehl Creek, it was less than 1.7 m and could have been associated with the 1410–1660 C.E. Ukiah surface rupture. The far-field geodetically determined slip rate for the

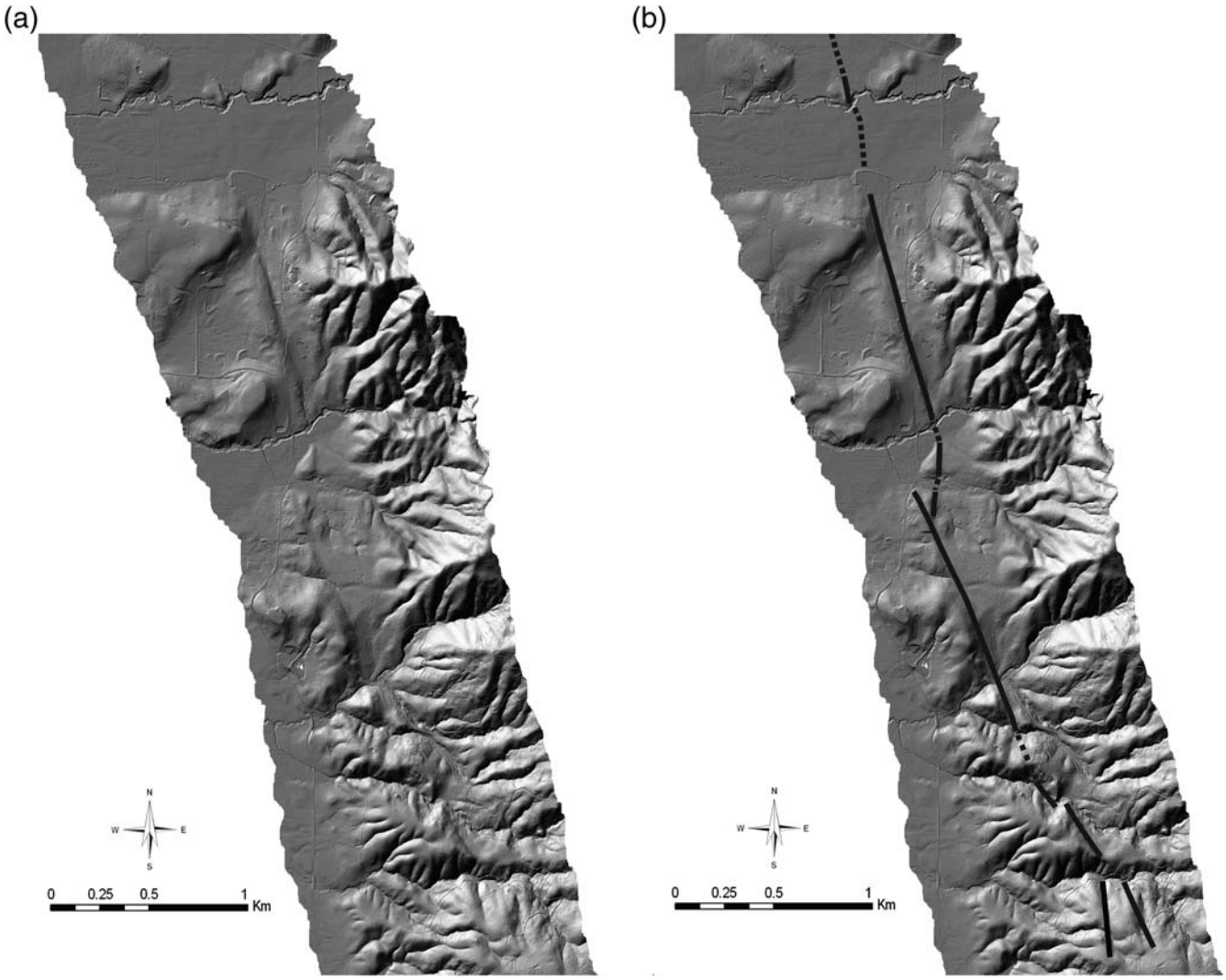

Figure 13. Hillshade produced from a filtered DEM derived from EarthScope Light Detection and Ranging (LiDAR) data, showing landforms indicative of Quaternary activity on a section of the East Willits fault: (left) image without annotation and (right) image with heavy lines showing our interpretation of East Willits fault traces. The location is given in Figure 2a.

Maacama fault is about twice the measured late Holocene slip rate at the Haehl Creek site, which leaves open the possibility of late Holocene earthquakes on other strands of the Maacama fault zone in addition to the strand investigated at Haehl Creek. Considering all of the possible scenarios allowed by the data, most lead to the conclusion that significant strain has accumulated across the fault that will be released as a future large earthquake. While additional work is needed to better constrain the fault's behavior and the relationships among creep rate, long-term geologic slip rate and geodetic slip rate, available evidence suggests that a large earthquake is expected to occur on this fault in the Willits area.

Data and Resources

The radiocarbon calibration program, CALIB 6.0, by Stuiver and Reimer, 1993 (v. 6), is available online at http://radiocarbon.pa.qub.ac.uk/calib/calib.html (last accessed September 2013). We rounded all calibrated age ranges to the nearest decade. The Light Detection and Ranging (LiDAR) data used to make the hillshade image shown in Figure 13 is available online at http://www.OpenTopography.org/data (last accessed September 2013).

All other data used in this paper are presented in the paper or electronic supplement or came from the published sources listed in the references.

Acknowledgments

We gratefully thank Margie Handley for providing access to the property to excavate trenches. We thank SHN Consulting Engineers & Geologists, Inc., especially Tom Stephens and Gary Simpson, for graciously sharing data from their earlier work at this site and helping to facilitate the permitting of this project, as well as for their insightful and helpful comments in the field. We also wish to thank Tom Herman for sharing survey data and for assistance of many kinds while we were in the field. We relied on the help of many volunteers and summer interns, in particular thanks to Gabriel Rothberg, Adam Woolace, Ryan Crawford, Julie Bawcom, and Emma Kelsey. Thanks to Scott

Haeffner, U.S. Geological Survey, for providing the kite aerial photogaphy used in Figures 5 and 10. Thanks also to Beda Garman and Bud Garman for their patience and skillful excavation of the trenches. We thank Pacific Gas & Electric Company for support for the radiocarbon dating. Helpful and constructive reviews of an early version of this manuscript were provided by Jesse Kass, Anne Sanquinni, Kate Scharer, and Jessica Murray. We thank reviewers Tim Dawson and Stéphane Baize for insightful and helpful reviews.

References

Castillo, D. A., and W. L. Ellsworth (1993). Seismotectonics of the San Andreas fault system between Point Arena and Cape Mendocino in northern California: Implications for the development and evolution of a young transform, *J. Geophys. Res.* **98,** no. B4, 6543–6560.

Erickson, G. (2008). Evolution of an intermontane basin along the Maacama fault, Little Lake Valley, northern California, *Master's Thesis*, Humboldt State University, Arcata, California, 109 pp.

Freymueller, J. T., M. H. Murray, P. Segall, and D. Castillo (1999). Kinematics of the Pacific-North America plate boundary zone, northern California, *J. Geophys. Res.* **104,** no. B4, 7419–7441.

Hay, E. A., N. T. Hall, and W. R. Cotton (1989). Rapid creep on the San Andreas fault at Bitterwater Valley, in *The San Andreas Transform Belt*, A. G. Sylvester and J. C. Crowell (Editors), *28th International Geological Congress*, Field Trip Guidebook T309, American Geophysical Union, Washington, D.C., 36–39.

Hayes, G. P., and K. P. Furlong (2006). The evolution of a plate boundary system—Crustal structure, seismicity and volcanism in northern California, *Seismol. Res. Lett.* **77,** no. 2, 201.

Hecker, S., and H. Kelsey (2006). History and pre-history of earthquakes in wine and redwood country, Sonoma and Mendocino Counties, California, in C. S. Prentice, J. G. Scotchmoor, E. M. Moores, and J. P. Kiland (Editors), *1906 San Francisco Earthquake Centennial Field Guides: Field Trips Associated with the 100th Anniversary Conference*, San Francisco, California, 18–23 April 2006, Geological Society of America, Field Guide 7, 339–372, doi: 10.1130/2006.1906SF(19).

Larsen, M. (2006). Late Holocene slip rate investigation of the Maacama fault at the Haehl Creek site, Willits, California, *Master's Thesis*, Humboldt State University, Arcata, California, 48 pp., 12 plates.

Lienkaemper, J. J., T. E. Dawson, S. F. Personius, G. G. Deitz, L. M. Reidy, and D. P. Schwartz (2002). A record of large earthquakes on the southern Hayward fault for the past 500 years, *Bull. Seismol. Soc. Am.* **92,** 2637–2658, doi: 10.1785/0120000611.

McFarland, F. S., J. J. Lienkaemper, and S. J. Caskey (2013). Data from theodolite measurements of creep rates on San Francisco Bay region faults, California: 1979-2012, *U.S. Geol. Surv. Open-File Rept. 2009-1119*, version 1.4, 18 pp.

Pampeyan, E. H., P. W. Harsh, and J. M. Coakley (1981). Preliminary map showing recently active breaks along the Maacama fault zone between Laytonville and Hopland, Mendocino County, California, *U.S. Geol. Surv. Misc. Field Studies, Map MF 5-11*, scale 1:24,000.

Prentice, C. S., P. Mann, L. Peña, and G. Burr (2003). Slip rate and earthquake recurrence along the central Septentrional fault, North American-Caribbean plate boundary, Dominican Republic, *J. Geophys. Res.* **108,** no. B3, 2149, doi: 10.1029/2001JB000442.

Reimer, P. J., M. G. L. Baillie, E. Bard, A. Bayliss, J. W. Beck, P. G. Blackwell, C. E. Buck, G. Burr, R. L. Edwards, M. Friedrich, *et al.* (2009). IntCal09 and Marine09 radiocarbon age calibration curves, 0–50,000 years cal BP, *Radiocarbon* **51,** no. 4, 1111–1150.

SHN Consulting Engineers & Geologists, Inc. (2004a). *Fault Rupture Hazard Evaluation*, Proposed Frank R Howard Memorial Hospital, APN 007-210-15, Willits, Mendocino County, California, 14 pp. (with figures and trench logs).

SHN Consulting Engineers & Geologists, Inc. (2004b). *Fault Rupture Hazard Evaluation*, Proposed Residential Subdivision, APN 007-250-27, Willits, Mendocino County, California, 15 pp. (with figures and trench logs).

Sickler, R. R., C. S. Prentice, and L. A. Dengler (2005). Slip rate and age of the most recent event on the central Maacama fault, near Ukiah, Mendocino County, California, abstract, *Geol. Soc. Am.* Abstracts with Programs, Paper No. 25-5, **37,** no. 4, 68 pp.

Stuiver, M., and P. J. Reimer (1993). Extended ^{14}C database and revised CALIB radiocarbon calibration program, *Radiocarbon* **35,** 215–230.

Toppozada, T. R., C. R. Real, and D. L. Parke (1981). Preparation of isoseismal maps and summaries of reported effects for pre-1900 California earthquakes, *Calif. Div. Mines Geol. Open-File Rept. 81-11 SAC*, 1–182.

Upp, R. R. (1989). Holocene activity and tectonic setting of the Maacama fault zone, Mendocino County, California, in *Richard H. Jahns Memorial Volume, Engineering Geology*, A. M. Johnson, C. W. Burnham, C. R. Allen, and W. Muehlberger (Editors), Vol. 27, Elsevier, Amsterdam, The Netherlands, 375–412.

Wells, D. L., and K. J. Coppersmith (1994). New empirical relationships among magnitude, rupture length, rupture width, rupture area and surface displacement, *Bull. Seismol. Soc. Am.* **84,** 974–1002.

Wesnousky, S. G., C. S. Prentice, and K. E. Sieh (1991). An offset Holocene stream channel and the rate of slip along the northern reach of the San Jacinto fault, San Bernardino, California, *Geol. Soc. Am. Bull.* **103,** 700–709.

Woolace, A. C. (2005). Late Neogene and Quaternary stratigraphy and structure of Little Lake Valley, northern Coast Range, California, *Master's Thesis*, Humboldt State University, Arcata, California, 59 pp.

U.S. Geological Survey
345 Middlefield Road MS 977
Menlo Park, California 94025
cprentice@usgs.gov
(C.S.P.)

Department of Geology
Humboldt State University
Arcata, California 95521
(M.C.L., H.M.K.)

URS Corporation
1333 Broadway, Suite 800
Oakland, California 94612-1924
(J.Z.)

Manuscript received 5 January 2014;
Published Online 21 October 2014